Front. Optoelectron. China 2008, 1(3–4): 231–236
DOI 10.1007/s12200-008-0072-7

RESEARCH ARTICLE

Four-core fiber-based bending sensor

Shigang ZHAO, Xue WANG, Libo YUAN (✉)

National University Science Park, Harbin Engineering University, Harbin 150001, China
Department of Physics, Harbin Engineering University, Harbin 150001, China

Abstract A novel four-core fiber-based bending sensor has been proposed. The four-core fiber is used as the sensing element, the four cores of the fiber act as a four-beam interferometer, and the far-field interferogram grids with periodical distributions are formed on the fiber output end. Since the phase difference is a function of the radius of curvature, the change of the radius of curvature shifts the far-field interferometric grid pattern. A low-coherence laser diode with wavelength of 650 nm is adopted to illuminate the fiber, and the interferogram pattern in the far-field is recorded by a CCD camera. The relationship between the far-field grid pattern intensity distribution and the radius of curvature is established theoretically and confirmed experimentally.

Keywords fiber optics, four-core fiber, bending sensor, far field, grid pattern

1 Introduction

Although many structures should ideally be rigid, performance is limited by deformation due to loading. Corrective action can usually be taken if the deformation is known. For example, "smart structures" have demonstrated the use of actuators to compensate for unwanted shape changes [1]. In continuous structures, changes in length due to uniform strain and thermal expansion can be significant. However, most of the variations in the overall shape are due to bending, and torsion creates a need for sensors specially optimized for the measurement of bending and twisting. Bending a beam produces a linear gradient in strain through the thickness of the beam. Local curvature can then be derived from the difference in strain between two strain gauges fixed to opposite sides of the beam; this is the basic type of electrical goniometer [2–4]. Fiber optic strain gauges are now well-established [5,6], and bending sensors based on two-mode fiber [7], multi-core fiber photonic crystal fiber [8,9] and multi-core Bragg gratings [10] are also proposed. They can be made by adhering two fiber optic strain sensors to either side of a flexible member [6], or embedding them both in the member.

In this paper, a four-core fiber-based four-beam fiber interferometer has been proposed and demonstrated. The four-core interferometer can automatically compensate the effect of temperature. The four-core fiber acts as a four-beam interferometer in which phase differences are a function of curvature. In the plane, containing the cores results in the shift of the far-field interferometric grid pattern.

Translated and revised from *Acta Optica Sinica*, 2006, 26(7): 1001–1006 [译自: 光学学报]

E-mail: lbyuan@vip.sina.com

2 Theory model of sensor

The proposed multi-parameter measurement approach is based on a sensing element formed from a four-core fiber, where the sensing element is manufactured by stacking identical silica rods with refractive index n_1 in a hexagonal array around four silica rods. These rods are located in every corner of a square, with higher refractive index n_2, then draws the bundle into a fiber. All of the silica rods with index n_1 fuse together to form an effective low-index cladding with light propagation in the effective high-index region associated with the four cores, as shown in Fig. 1. The unusual structure of the single mode four-core fiber leads to the novel waveguide properties. In particular, an interferometric grid far-field pattern can be formed at the output end of the four-core single mode fiber.

To analyze the phase differences resulting from the bending of four-core fiber and determine the relationship between every parameter, the coordinate diagram is established as shown in Fig. 2.

In Fig. 2 the bending fiber is in the plane Y-Z, and all of the parameters are related with the optical phase differential of every core to the centre of the four-core fiber, i.e.,

$$\delta\phi_m = k_0 nL\left(\frac{\delta n_m}{n} + \frac{\delta L_m}{L}\right) \quad (m = 1,2,3,4), \qquad (1)$$

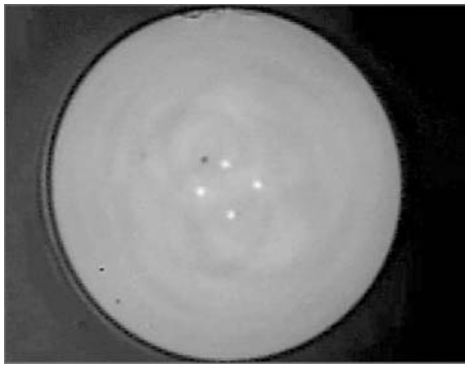

Fig. 1 Four-core fiber acting as a bending sensor

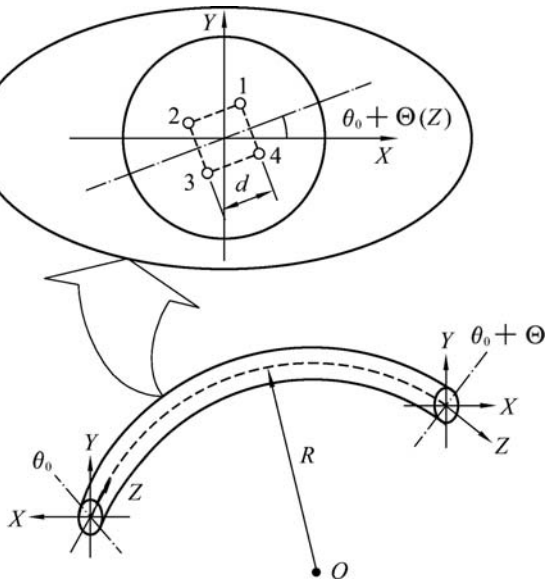

Fig. 2 Coordinate diagram to calculate phase difference of bended four-core fiber

where k_0 is the wave number and n is the refractive index of the fiber core; L represents the length of the four-core fiber; and δn_m and δL_m represent the index and core length differences between core m and the fiber center, respectively. In Eq. (1), the term $\delta L_m/L$ corresponding to the main strain component is along Z and is given by

$$\varepsilon_z = \frac{\delta L_m}{L} = \frac{x_m}{R} \quad (m=1,2,3,4), \tag{2}$$

where R is the curvature of the four-core fiber. The term x_m is the projection distance in X axis from the core m to the center of the fiber, and is determined by

$$x_m = \frac{\sqrt{2}d}{2}\cos\left[\theta_0+(2m-1)\frac{\pi}{4}+\theta(z)\right] \quad (m=1,2,3,4), \tag{3}$$

where d is the distance of the neighbor cores, θ_0 is the initial orientation angle of the four-core as shown in Fig. 2, and $\theta(z)$ is the twisting angle along the fiber axis Z. The variations of the index by bending can be expressed as [11]

$$\delta n(m) \approx \delta n_x(m) \approx \delta n_y(m) \approx -c_2\frac{n^3}{2}\frac{x_m}{R} \quad (m=1,2,3,4), \tag{4}$$

where $c_2 = 0.204$ is a constant.

The changes of phase difference by bending are given below

$$\delta\phi_m = \frac{\sqrt{2}k_0nLd}{2R}\left(1-c_2\frac{n^2}{2}\right)\cos\left[\theta_0+(2m-1)\frac{\pi}{4}+\theta(z)\right]. \tag{5}$$

For the case of twisting a smaller angle, the linear dependence of the twisting angle $\theta(z)$ along the fiber can be simply expressed as

$$\theta(z) = \frac{\Theta}{L}z, \tag{6}$$

where Θ is the net rotation angle as observed at the exit of the fiber end. With the curvature radius R, the phase difference by bending and twisting can be expressed as

$$\begin{aligned}\Delta\phi_m &= \frac{\sqrt{2}k_0nLd}{2R}\left(1-c_2\frac{n^2}{2}\right)\cos\left[\theta_0+(2m-1)\frac{\pi}{4}+\Theta\right]\\ &= \xi\frac{L}{R}\cos\left[\theta_0+(2m-1)\frac{\pi}{4}+\Theta\right],\end{aligned} \tag{7}$$

where ξ is a constant, substitute $k_0 = 2\pi/\lambda$, $\lambda = 0.65\,\mu$m, $n = 1.46$, $d = 18\,\mu$m and $c_2 = 0.204$ into Eq. (7), which gives

$$\xi = \frac{\sqrt{2}k_0nd}{2}\left(1-c_2\frac{n^2}{2}\right) = 140.46. \tag{8}$$

The length of the four-core fiber L is known as the azimuth angle of the fiber end, and the curvature radius R is the function of phase difference.

The space between four cores of the four-core fiber is as small as 18 μm. The optical power in every core is equal with the same light source. Thus, the intensity distribution in the observation plane can be written as [12,13]

$$\begin{aligned}I(u,v) = 4I_0[&1+\cos(\psi_1-\psi_2)\cos(\phi_1-\phi_2)\\ &+\cos(\psi_1-\psi_3)\cos(\phi_1-\phi_3)\\ &+\cos(\psi_1-\psi_4)\cos(\phi_1-\phi_4)\\ &+\cos(\psi_2-\psi_3)\cos(\phi_2-\phi_3)\\ &+\cos(\psi_2-\psi_4)\cos(\phi_2-\phi_4)\\ &+\cos(\psi_3-\psi_4)\cos(\phi_3-\phi_4)],\end{aligned} \tag{9}$$

where ψ_m is the angle between the polarized direction and X axis, as shown in Fig. 3(c). $(\phi_k - \phi_m)$ is the total phase difference between random two cores and is expressed as

$$\begin{aligned}\phi_k-\phi_m = k_0(l_k-l_m)+(\delta\phi_k-\delta\phi_m)\\ (k,m=1,2,3,4),\end{aligned} \tag{10}$$

where l_m $(m = 1,2,3,4)$ is the distance between fiber m and observation plane as shown below:

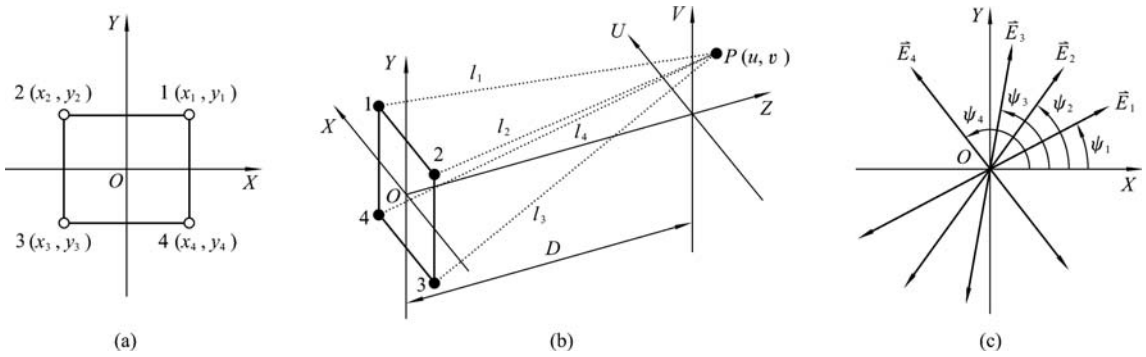

Fig. 3 Far-field coordinate system of output end of four-core fiber. (a) Core positions on the end of the fiber; (b) relationship between output plane lie in the end of the fiber and the observation plane; (c) polarization states in the output end of the fiber

$$l_m = \left[(u-x_m)^2 + (v-y_m)^2 + D^2\right]^{1/2}. \tag{11}$$

For the condition of the far-field, $(u, v) \gg (x, y)_{\max}$, Eq. (11) can be estimated as

$$l_m \approx D\left(1 - \frac{ux_m + vy_m}{D}\right). \tag{12}$$

Eq. (10) could be written more conveniently as

$$\phi_k - \phi_m = \frac{k_0}{D}[u(x_m - x_k) + v(y_m - y_k)] + (\delta\phi_k - \delta\phi_m) \quad (k,m = 1,2,3,4), \tag{13}$$

x_m is given by Eq. (3). y_m is the projection distance in Y axis from the core m to the center of the fiber, and it is given below:

$$y_m = \frac{\sqrt{2}d}{2}\sin\left[\theta_0 + (2m-1)\frac{\pi}{4} + \theta(z)\right] \quad (m = 1,2,3,4). \tag{14}$$

In the experiment, adjusting the polarization states and twisting the output end can eliminate the interferometer between core (1, 3) and core (2, 4), and the terms of core (1, 2), (3, 4) and (1, 4), (2, 3) are combined. Thus, Eq. (9) can be simplified as

$$I(u,v) = 4I_0[1 + 2\zeta_1\cos(\phi_1 - \phi_2) + 2\zeta_2\cos(\phi_1 - \phi_4)], \tag{15}$$

where $\zeta_1 = \cos(\psi_1 - \psi_2)$ and $\zeta_2 = \cos(\psi_1 - \psi_4)$ are the constants less than 1. Substituting Eqs. (3), (8), (13) and (14) into Eq. (15), the relationship between the far-field interferometric grid pattern and the fiber curvature R is given below:

$$I(u,v) = 4I_0\left\{1 + 2\zeta_1\cos\left\{\frac{k_0 d}{D}[u\cos(\theta_0+\Theta) - v\sin(\theta_0+\Theta)] - \sqrt{2}\xi\frac{L}{R}\cos(\theta_0+\Theta)\right\} + 2\zeta_2\cos\left\{\frac{k_0 d}{D}[u\cos(\theta_0+\Theta) - v\sin(\theta_0+\Theta)] - \sqrt{2}\xi\frac{L}{R}\sin(\theta_0+\Theta)\right\}\right\}. \tag{16}$$

It can be seen from Eq. (16) that the fiber curvature R is parallel with the space moving of light-field $I(u,v)$. The linearity relationship is shown below:

$$\rho = \frac{k_0 d}{\xi L D}[u - v\tan(\theta_0 + \Theta)] + C. \tag{17}$$

Since every core of the four-core fiber is single mode, the intensity distribution I_0 can be approximately expressed as an individual Gaussian distribution [14], i.e.,

$$I_0 = G_0\exp\left\{-\frac{(u^2+v^2)}{\omega_0{}^2\left[1+\eta(D/\omega_0)^{3/2}\right]^2}\right\}, \tag{18}$$

where G_0 represents scale constant, $\eta = 0.81 \times 10^{-7}$ is a dimensionless parameter related to the fiber NA, and $\omega_0 = 1.9\,\mu$m is the radius of the single mode for every core of the four-core fiber. The distance between the output fiber end and the CCD detection surface was measured as $D = 3$ mm, as shown in Fig. 4(a). Substituting Eq. (18) into Eq. (16) and selecting $\theta_0 = \Theta = 0$, the output far-field fringe patterns from experimental results are shown in Fig. 4(b), similar with the result in Fig. 4(c) by Eq. (16).

3 Relationship between experimental setup and sensing characteristics

The four-core fiber with sensing length $L = 15$ cm was embedded in the strain-free neutral axis between the two elastic steel plates. A three-point beam bending experiment was undertaken as shown in Fig. 5.

In the experiment, the span width of the specimen two supporting points $L_{AB} = 12$ cm, and express the midpoint of the elastic steel plate with a screw micrometer by 2 mm for one step, until $L_{CD} = 12$ mm, in Fig. 5(b) it can be seen that

$$R = \frac{4(L_{CD})^2 + 12^2}{8L_{CD}}\ (\text{cm}). \tag{19}$$

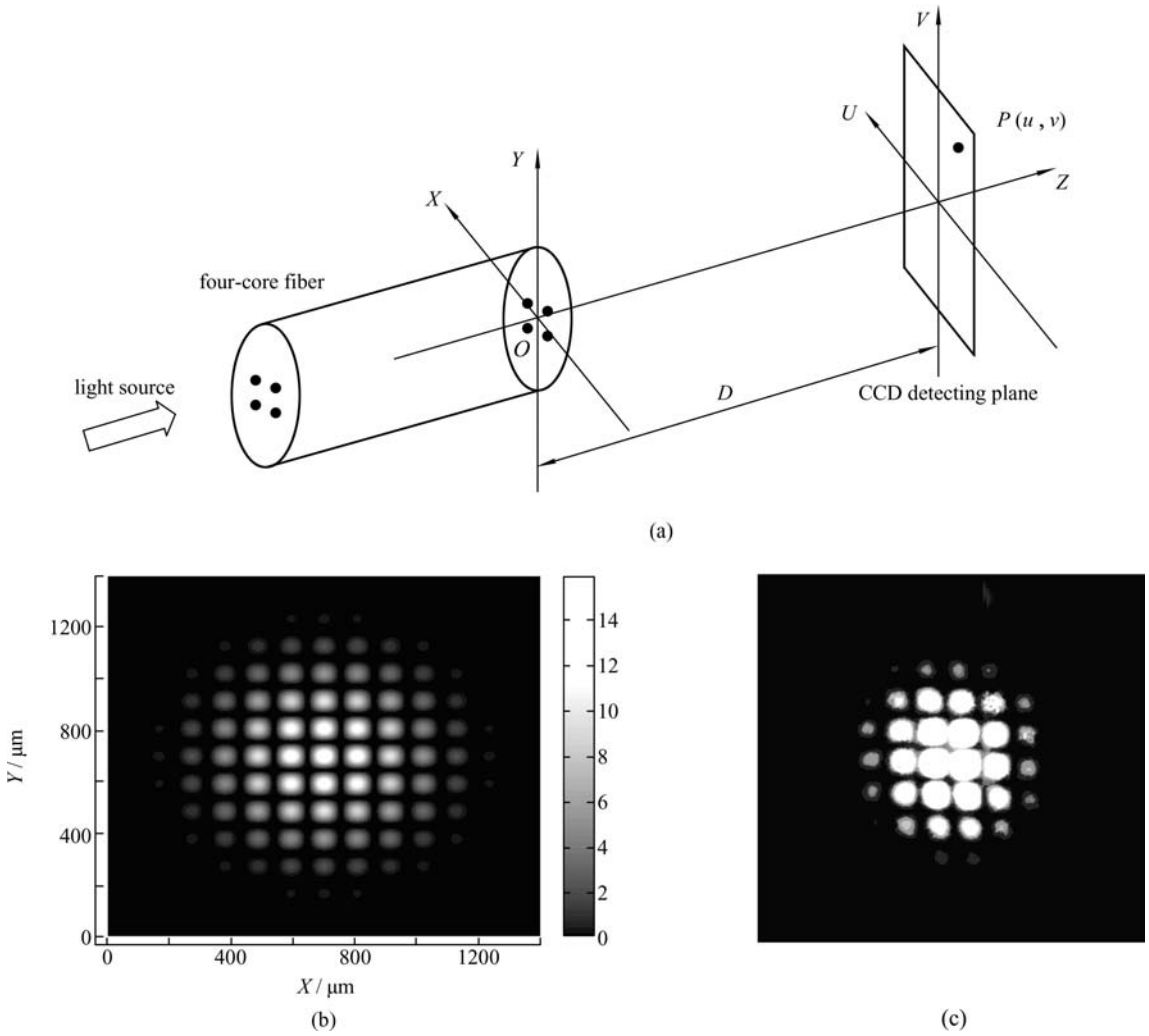

Fig. 4 Four-core fiber output far-field fringe patterns. (a) Experimental set-up; (b) theoretical simulation result; (c) experimental result

The relationship between the deflection L_{CD} and the curvature $(1/R)$ for the three point bending beam is shown in Fig. 6. It can be seen that the relationship between ρ and L_{CD} is linear.

4 Experimental results and discussions

The far-field interferometric grid pattern is recorded by a CCD camera, as shown in Fig. 7(a). It can be measured

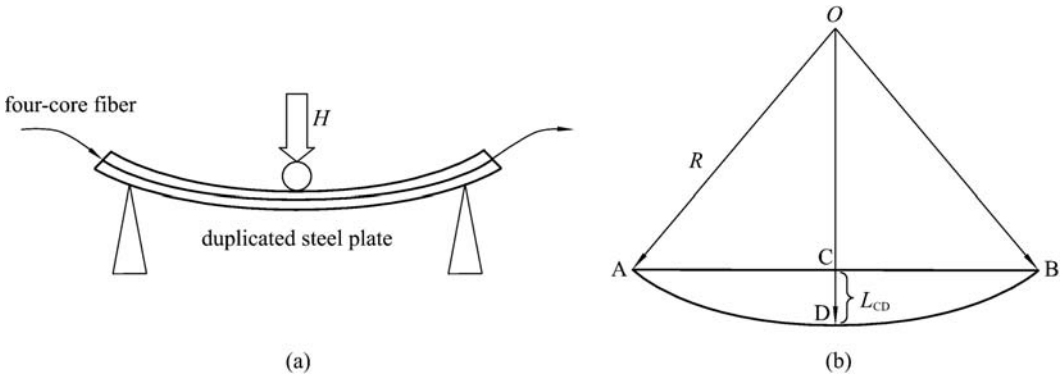

Fig. 5 Three-point bending beam experimental set-up with four-core fiber embedded in neutrality layer. (a) Experimental set-up of three-point bending beam; (b) schematic plan of geometrical sizes

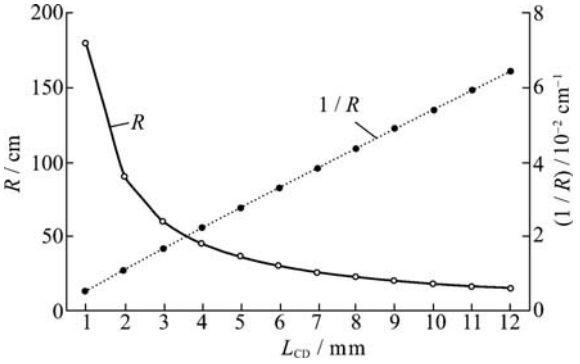

Fig. 6 Relationship between deflection L_{CD} and curvature ($1/R$) for three-point bending beam

that the twisting angle $\theta_0+\Theta=71.5^\circ$, and the measurement process is shown in Fig. 7(b). The measurements of L_{CD} and the moving curve by U, V axis are given in Fig. 8(a).

Figure 8(b) shows the relationship between the deflection L_{CD} and the curvature ($1/R$). It can be seen that the experimental result is in agreement with the theoretical prediction, and it also has some deviation.

In fact, the polarization states may take some effects to the measuring process. With the curvature radius reducing, the double-efraction effect in every core is increasing. Since this effect and the main change are independent, we have

$$\Delta\delta n=\delta n_x-\delta n_y=(c_2-c_1)\frac{n^3}{4R^2}\left(x_m^2-r^2\right), \qquad (20)$$

where $c_1=0.075$ and r is the fiber radius. Although the difference is small, the effect of the output field is by the change of polarization states ψ_m ($m=1,2,3,4$). With the special four-core fiber, in which four cores centralize with each other, this effect is small.

5 Conclusions

A four-core fiber has been designed and used as a four-beam in-fiber integrated interferometer. The sensing char-

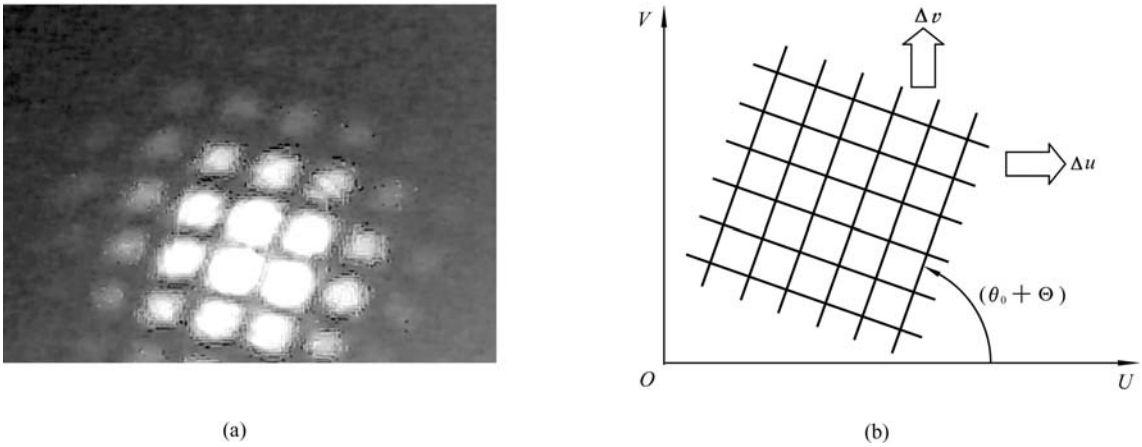

Fig. 7 Far-field interferometric grid pattern and its measuring approach. (a) Far-field fringe pattern from CCD; (b) measuring method of integral shift of grid pattern

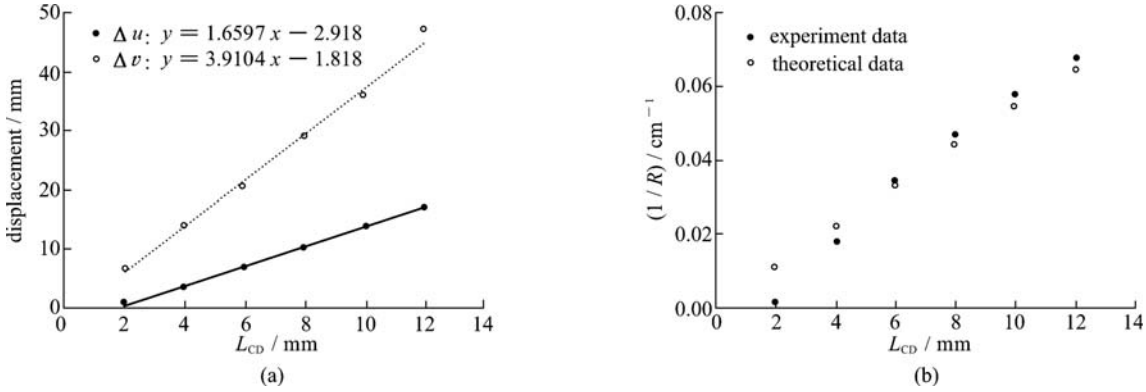

Fig. 8 Experimental results and theoretical prediction. (a) Measuring results of L_{CD} and the shift of grid pattern; (b) comparison between experimental data and theoretical prediction

acteristics of curvature have been investigated. The experimental results show that the four-core fiber could be used as multi-parameter sensors and has the potential applications in smart structural condition monitoring.

Acknowledgements This work was supported by the National Natural Science Foundation of China (Grant No. 60577005) and the Teaching and Research Award Program for Outstanding Young Professors in Higher Education Institute, MOE, P. R. C., to Harbin Engineering University.

References

1. Culshaw B. Smart Structures and Materials. Boston: Artech House, 1996, 1–15
2. Zhou X J, Gong J J, Liu Y Z, et al. Analysis of white-light interference distributed optic fiber sensor by polarized modes coupling. Acta Optica Sinica, 2004, 24(5): 605–608 (in Chinese)
3. Xiong S D, Luo H, Hu Y M et al. Research on interferometric polarization maintaining fiber optic micro-vibration vector sensor. Chinese Journal of Lasers, 2004, 31(7): 843–847 (in Chinese)
4. Xiong L Y, Kai G Y, Sun L, et al. Dual wavelength erbium-doped fiber laser with a lateral pressure-tuned Hi-Bi fiber Bragg grating. Chinese Optics Letters, 2004, 2(12): 686–687
5. Jackson D A. Recent progress in monomode fibre-optic sensors. Measurement Science and Technology, 1994, 5(6): 621–638
6. Xu M G, Archambault J L, Reekie L, et al. Thermally-compensted bending gauge using surface-mounted fiber gratings. International Journal of Optoelectronics, 1994, 9(3): 281–283
7. Covington C E, Blake J, Carrara S L A. Two-mode fiber-optic bending sensor with temperature and strain compensation. Optics Letters, 1994, 19(9): 676–678
8. Gander M J, Galliot E A C, McBride R, et al. Bend measurement using mutli-core optical fiber. In: Proceedings of 12th International Conference on Optical Fiber Sensors, 1997, 166–169
9. Gander M J, Macrae D, Galliot E A C, et al. Two-axis bend measurement using multicore optical fibre. Optics Communications, 2000, 182(1–3): 115–121
10. Gander M J, MacPherson W N, McBride R, et al. Bend measurement using Bragg gratings in multicore fibre. Electronics Letters, 2000, 36(2): 120–121
11. Vallee R, Drolet D. Practical coupling device based on a two-core optical fiber. Applied Optics, 1994, 33(24): 5602–5610
12. Yuan L B. Fiber-optic Moiré interferometer. Chinese Physics Letters, 1997, 14(9): 675–677
13. Yuan L B, Zhou L M. Fiber optic Moiré interference principle. Optical Fiber Technology, 1998, 4(2): 224–232
14. Yuan L B, Liu Q A, Zhao Q W. The output optical field intensity distribution formed by an optical fiber end. Optical Communication Technology, 1995, 19(2): 159–161